Electronic Supplementary Material (ESI) for Journal of Materials Chemistry A.

Supporting Information

Enhancing Electrochemical Nitrogen Reduction of Ru Nanowire by Atomic Decoration of Pt

Weiqing Zhang[a,b] *Liting Yang,*[b] *Changhua An,*[b,]* *Jichao Zhang,*[c] *JunFa Zhu,*[d,]* *Peng Chen*[a,]*

[a]School of Chemical and Biomedical Engineering, Nanyang Technological University, Singapore 637457, Singapore

[b]Tianjin Key Laboratory of Advanced Functional Porous Materials, Institute for New Energy Materials & Low-Carbon Technologies, Tianjin University of Technology, Tianjin 300384, China

[c]Shanghai Synchrotron Radiation Facility, Shanghai Institute of Applied Physics, Chinese Academy of Sciences, Shanghai, 201204, China

[d]National Synchrotron Radiation Laboratory, University of Science and Technology of China, Hefei, Anhui 230029, China

E-mail: chenpeng@ntu.edu.sg, anch@tjut.edu.cn, jfzhu@ustc.edu.cn

EXPERIMENTAL SECTION

Chemicals.

Ruthenium chloride hydrate ($RuCl_3 \cdot xH_2O$), sodium hydroxide ($NaOH$), salicylic acid ($C_7H_6O_3$), sodium nitroferricyanide dihydrate ($C_5FeN_6Na_2O$ $2H_2O$) and 4-(dimethylamino) benzaldehyde ($C_9H_{11}NO$) were purchased from Aladdin; hydrogen hexachloroplatinate (IV) hydrate (H_2PtCl_6) was bought from ACROS; poly(vinylpyrrolidone) (PVP, MW~40,000) were purchased from Aldrich; sodium n-dodecyl sulfate (SDS), potassium fluoride (KF), sodium bromide (NaBr), phenol (C_6H_5OH), ammonium chloride (NH_4Cl), ethanol (C_2H_5OH), hydrazine hydrate ($N_2H_4 \cdot H_2O$, 85.0%), potassium chloride (KCl), and potassium hydroxide (KOH) were purchased from Sinopharm Chemical Reagent Co. Ltd.; sodium hypochlorite solution (NaClO, available chlorine 4%) was purchased from Shanghai Macklin Biochemical Co. Ltd.; Nessler's reagent ($K_2[HgI_4]$, analytical grade) and potassium sodium tartrate tetrahydrate ($NaKC_4H_4O_6 \cdot 4H_2O$, 99.0%) were purchased from Tianjin Guangfu Technology Development Co. Ltd.; $^{15}N_2$ (^{15}N>99.0 atom%) were purchased from the Shanghai Research Institute of Chemical Industry Co. Ltd; N_2 (N_2>99.999%, ^{15}N=0.36 atom%) were purchased from Tianjin Huanyu Gas Co. Ltd. The ultrapure water was used in all the experiments with a specific resistance of 18.2 MΩ·cm.

Characterizations.

The morphology, structure, and composition of the samples were examined with transmission electron microscopy (TEM/EDX, TECNAI G2 Spirit TWIN, 200 kV), high-resolution TEM and selected area electron diffraction (HRTEM/SAED/EDX, TALOS F200 X, 200 kV). Atom-resolution HAADF images were obtained with a transmission electron microscope equipped with a probe corrector (Titan Cubed Themis G2 60-300, FEI). The extended X-ray fine structure (EXAFS) analysis was performed on the BL14W1 beamline of Shanghai Synchrotron Radiation Facility. The spectra were obtained from 13,400 to 13,480 eV in solid-state detector mode with 0.5 eV steps at the near edge. X-ray diffraction (XRD) patterns were obtained by MiniFlex600 with Cu-Kα radiation. X-Ray photoelectron spectroscopy (XPS) was performed by a X-ray photoelectron spectrometer (ESCALAB250Xi) with a pass energy of 20.00 eV and an Al Kα excitation source (1486.6 eV). The atomic ratio of the sample was determined by ICP-MS (Thermo Fisher Scientific, iCAP RQ). The concentration of ^{15}N isotope-labeling products was established by isotopic mass spectrometry (MAT-271).

Synthesis of $Ru_{76}Pt_{24}$, and $Ru_{47}Pt_{53}$, Ru and Pt nanowires.

$Ru_{76}Pt_{24}$, $Ru_{47}Pt_{53}$, and Ru ultrathin nanowires were synthesized with the same method as for $Ru_{88}Pt_{12}$ nanowires except using different ratios of $RuCl_3/H_2PtCl_6$ (as shown in Table S2). Pt ultrathin nanowires were synthesized following the literature [ref 37 in main text]. Briefly, 128 mg of PVP, 435.2 mg of sodium dodecyl sulfonate, 164.8 mg of NaBr, and 0.8 mL of H_2PtCl_6 (0.1 M) were added to 15.2 mL of water under stirring. Then the aqueous solution was transferred to a 24 mL Teflon-lined stainless-steel autoclave, which was was then heated at 210 ℃ for 12 h.

Determination of NH_3 yield

The yield of NH_3 was spectrophotometrically determined by methods using phenate, Nessler's reagent, or indophenol [S1, ref 38 in the main text]. For the phenate-based method, 1 mL of 0.64 M C_6H_5OH, 0.38 M NaOH, and 1.3 mM $C_5FeN_6Na_2O$ solution was mixed with 1 mL of 55 mM NaClO solution (dissolved in 0.75 M NaOH). Then 1 mL of standard NH_4Cl solution (0, 0.2, 0.5, 0.8, 1.0, 1.2, 1.5, 2.0 ppm in 0.1 M KOH) was added to the above solution, followed by thorough mixing and keeping in dark for 30 min. UV-vis spectra were acquired and absorbance at 633 nm was taken to draw the calibration curve. For Nessler's reagent method, 4 mL of standard NH_4Cl solutions (0, 0.2, 0.5, 0.8, 1.0, 1.2, 1.5, or 2.0 ppm in 0.1 M KOH) were prepared. Then 1.0 mL of 0.2 M $NaKC_4H_4O_6$ solution and 0.15 mL Nessler's reagent were added. The resulting solution was kept in dark for 25 min after mixing thoroughly. UV-vis spectra were acquired and the absorbance at 425 nm was taken to draw the calibration curve. For indophenol blue method, 2.0 mL of 1.0 M NaOH containing 5 wt% $NaKC_4H_4O_6$ and 5 wt% $C_7H_6O_3$ was added into 2 mL standard NH_4Cl solutions, which was followed by adding 1.0 mL of 0.05 M NaClO solution (diluted by 0.75 M NaOH) and 0.2 mL of 1 wt% $C_5FeN_6Na_2O$ solution. Finally, the obtained solution was mixed thoroughly and kept in dark for 2 h. UV-vis spectra were acquired and absorbance at 655 nm was taken to draw the calibration curve. Electrolytes after ENRR were diluted for 5 times for the above colorimetric assays. Based on the obtained calibration curve, the yield of NH_4^+ can be determined.

Determination of hydrazine

The yield of hydrazine (N_2H_4) product was spectrophotometrically determined by the Watt and Chrisp method [ref 38 in the main text]. The chromogenic reagent was prepared by adding $C_9H_{11}NO$ (5.99 g) and concentrated HCl (30 mL) into 300 mL ethanol. 2.0 mL of standard N_2H_4 solutions (0, 0.2, 0.5, 1, 1.5, or 2.0 ppm in 0.1 M

KOH) were prepared. After adding 2.0 mL chromogenic reagent, the solution was mixed thoroughly and kept in dark for 20 min. UV-vis spectra were acquired and absorbance at 460 nm was taken to draw the calibration curve. N_2H_4 product in the electrolytes after ENRR was determined using the above colorimetric assay and based on the calibration curve.

Calculation of Faradaic efficiency.

The conversion of N_2 to NH_3 requires three electrons. The Faraday efficiency of the process is calculated based on Equation S1,

$$FE = 3F \times n(NH_3) \,/\, Q \qquad \text{Equation S1}$$

where F is the Faraday constant, Q is the electrical charge, and n is the total molar weight of NH_3, respectively.

Theoretical calculations.

First-principles calculations were conducted using the Vienna Ab-Initio Simulation Package [S2,S3]. The Perdew-Burke-Ernzerhof functional of flavor generalized gradient approximation was adopted for the exchange–correlation potential [S4]. Van der Waals correction of Grimme scheme (D2) was included to improve the description of the dispersion interaction between adsorbates and substrates [S5,S6]. The vacuum thickness in the z direction was set to be >15 Å to avoid unphysical interactions between periodic images. The bimetallic PtRu(111) surface was modeled by five-layer (3 × 3) Ru(111) cell with one surface Ru atom replaced by a Pt atom (see Fig. S25 and S26). A gamma-centered 5 × 5 × 1 grid was employed for the Brillouin-zone sampling with a plane-wave cutoff energy of 500 eV. The adsorption energies of X (X = N_2, N_2H and

H) on surfaces were calculated as

$$\Delta E_X = E_{*X} - E_{*} - E_{N_2} - \frac{n}{2} E_{H_2}.$$

E_{*X} and E_{*} are the total energies of surface with and without adsorbed X, respectively. E_{N_2} and E_{H_2} are the total energies of N_2 and H_2 molecules in gas phase, respectively. *n* equals to 0 if X is N_2, while is 1 when X = N_2H and H.

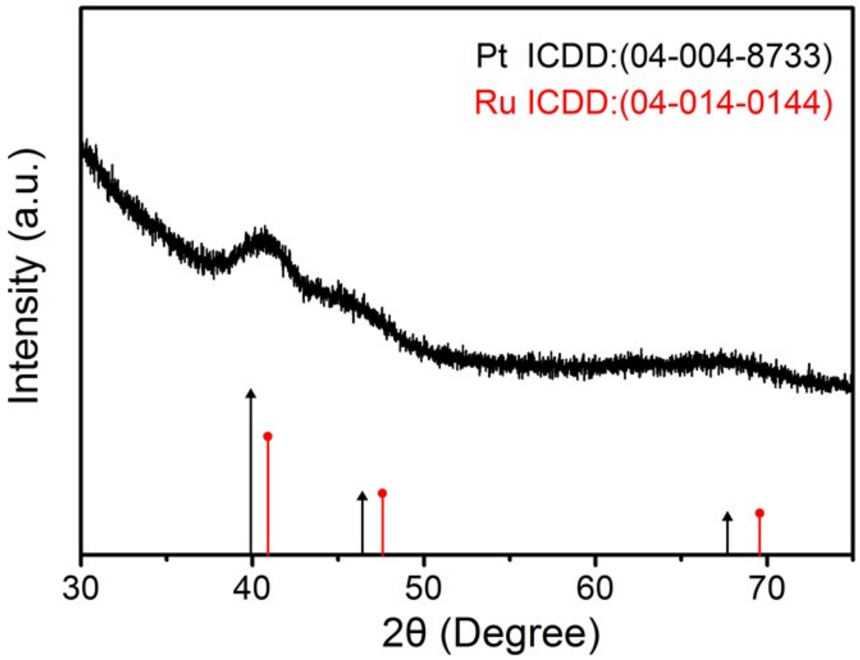

Fig. S1. XRD patterns of $Ru_{88}Pt_{12}$ nanowires. The black and red lines indicate to the peak positions of pure Pt (ICDD:04-004-8733) and Ru (ICDD:04-014-0144).

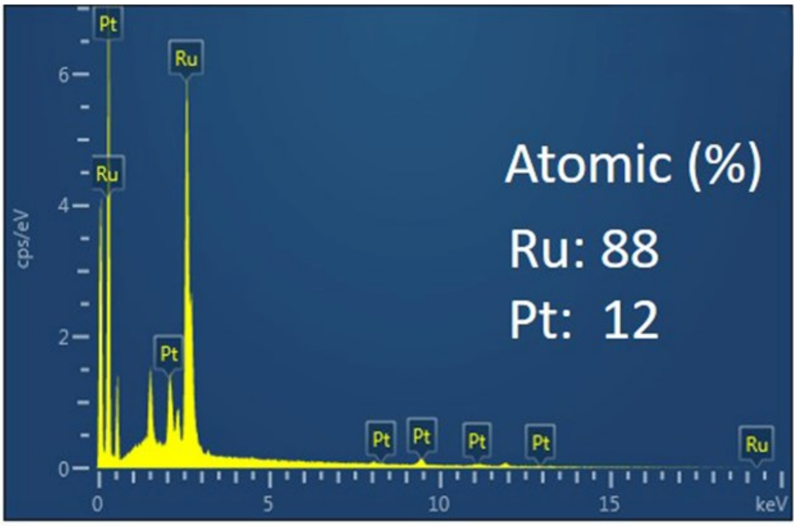

Fig. S2. The energy dispersive X-ray spectroscopy (EDS) of $Ru_{88}Pt_{12}$ nanowires.

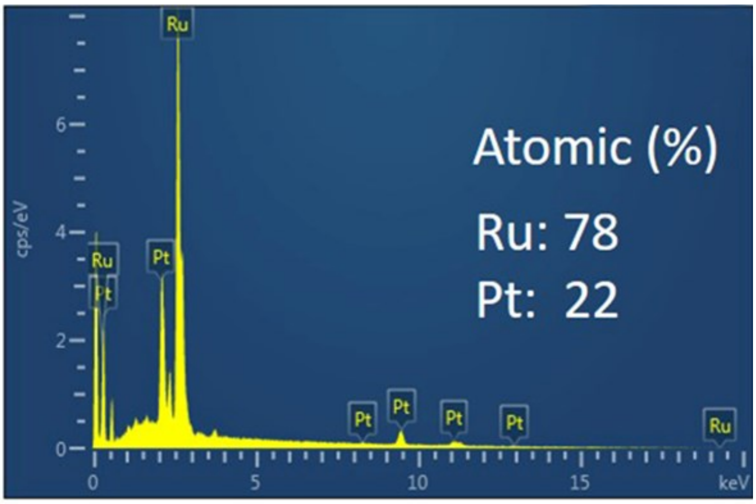

Fig. S3. The energy dispersive X-ray spectroscopy (EDS) of $Ru_{76}Pt_{24}$ nanowires.

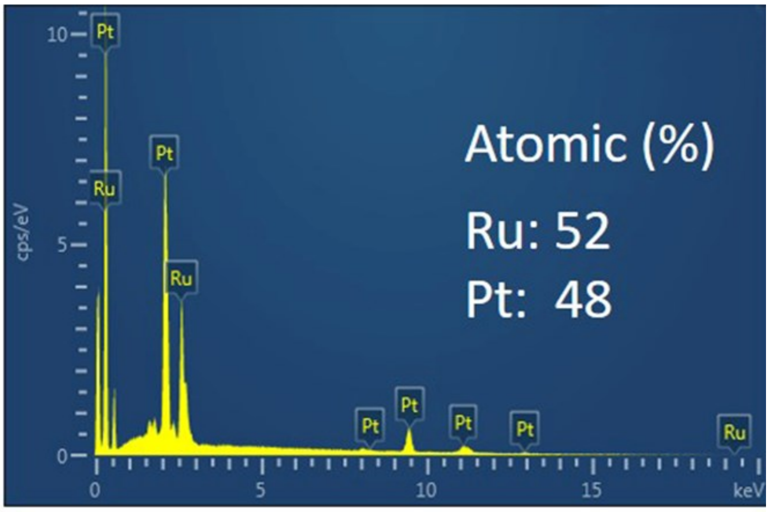

Fig. S4. The energy dispersive X-ray spectroscopy (EDS) of $Ru_{47}Pt_{53}$ nanowires.

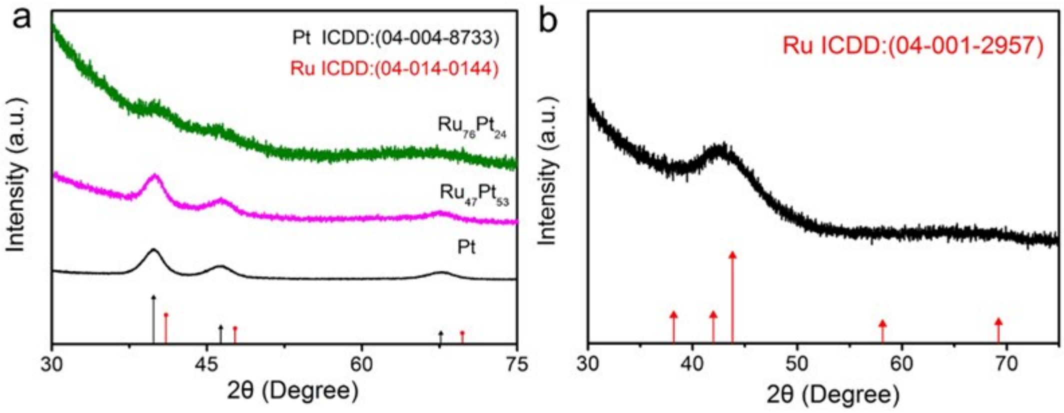

Fig. S5. (a) XRD patterns of $Ru_{76}Pt_{24}$, $Ru_{47}Pt_{53}$, and Pt nanowires. The black and red lines indicate the peak positions of *fcc* Pt (ICDD:04-004-8733) and Ru (ICDD:04-014-0144). (b) XRD of Ru nanowires. The red lines indicate the peak positions of *hcp* (ICDD:04-001-2957).

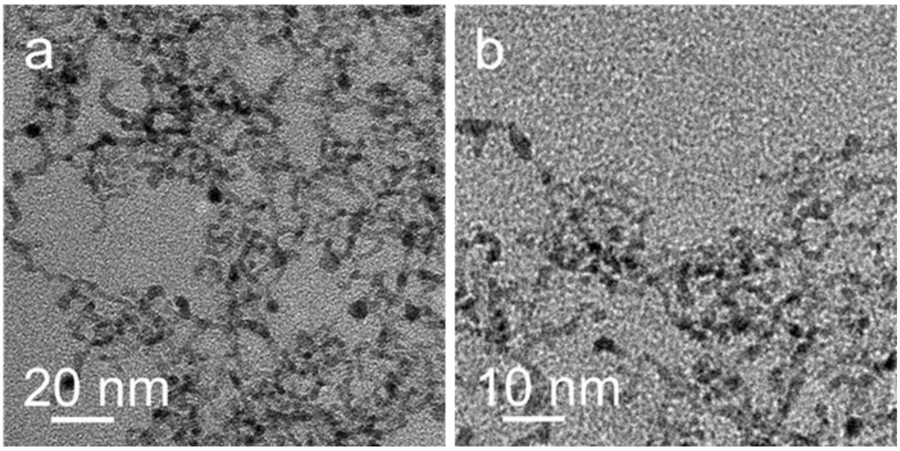

Fig. S6. TEM images of $Ru_{76}Pt_{24}$ nanowires.

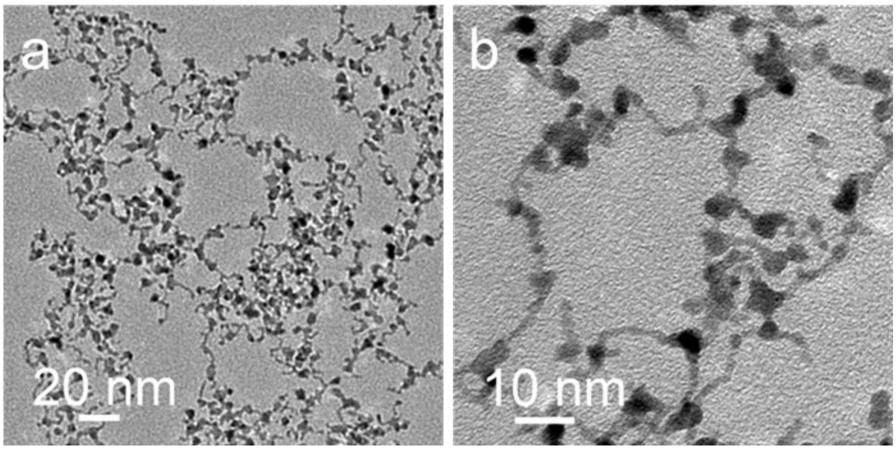

Fig. S7. TEM images of $Ru_{47}Pt_{53}$ nanowires.

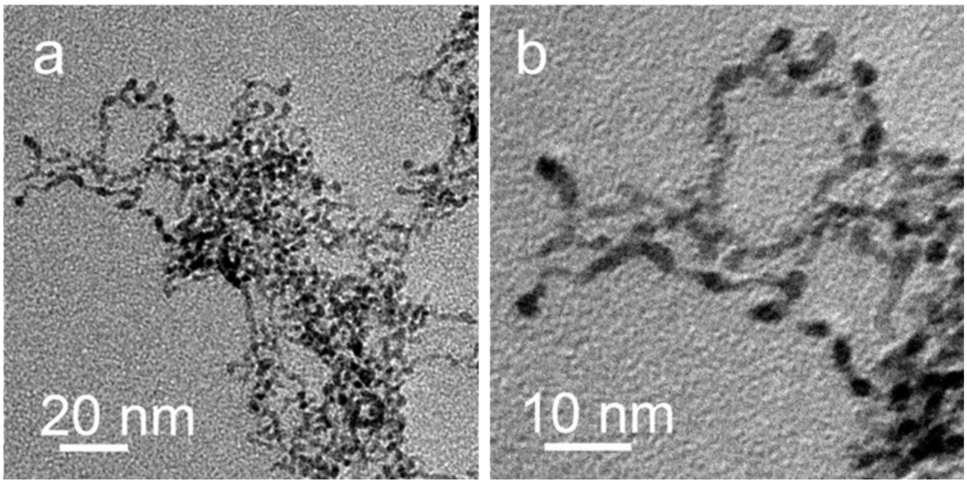

Fig. S8. TEM images of Ru nanowires.

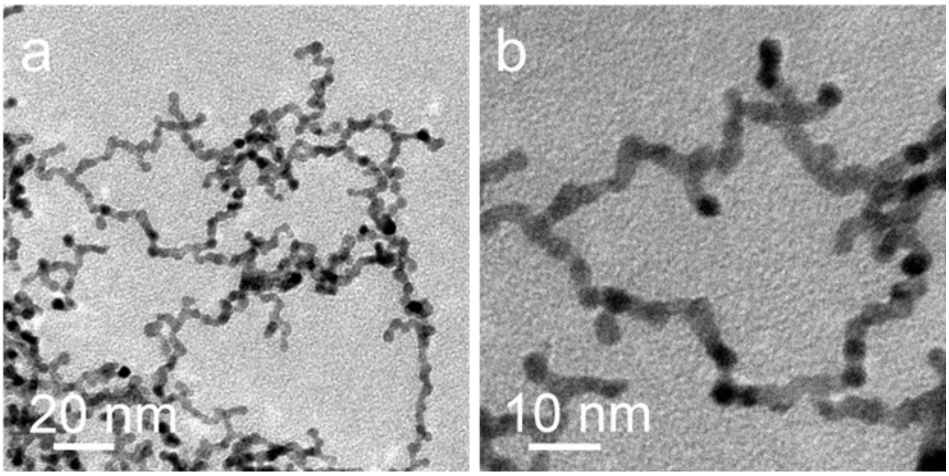

Fig. S9. TEM images of Pt nanowires.

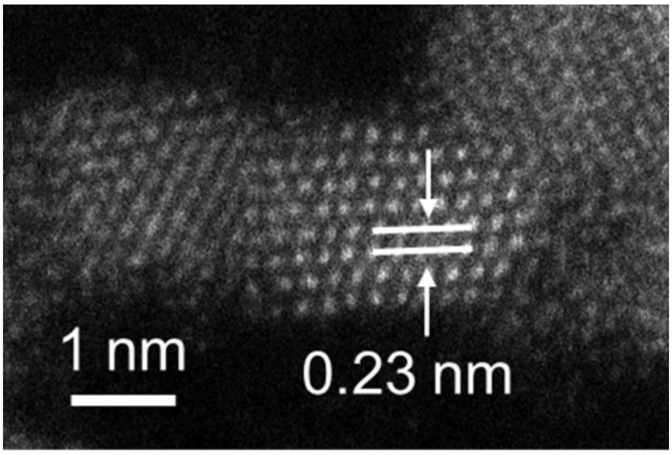

Fig. S10. HRTEM image of Pt enriched domain on a $Ru_{88}Pt_{12}$ nanowires.

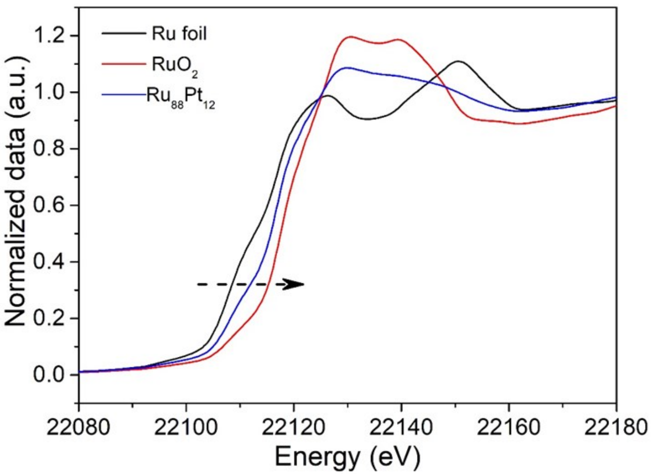

Fig. S11. Ru K-edge EXAFS spectra of $Ru_{88}Pt_{12}$ nanowires with reference to Ru foil and RuO_2.

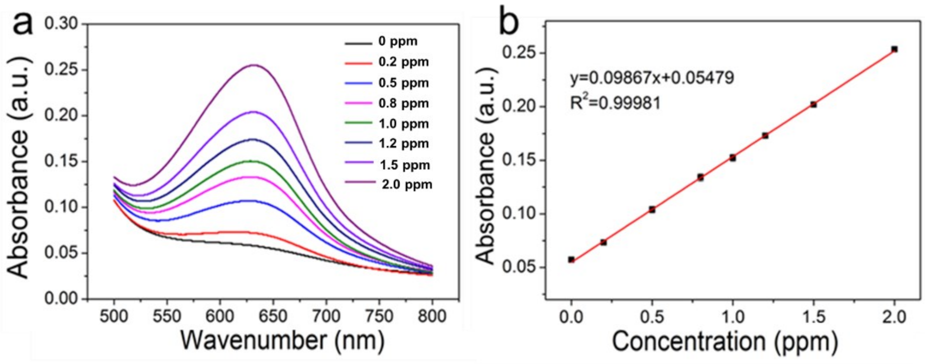

Fig. S12. (a) UV-vis curves of NH_4^+ standard solutions colored with phenate after keeping in dark for 30 min at room temperature. (b) Calibration curve. The UV-Vis spectra were measured for three times and the average absorbance at 633 nm was taken to draw the curve.

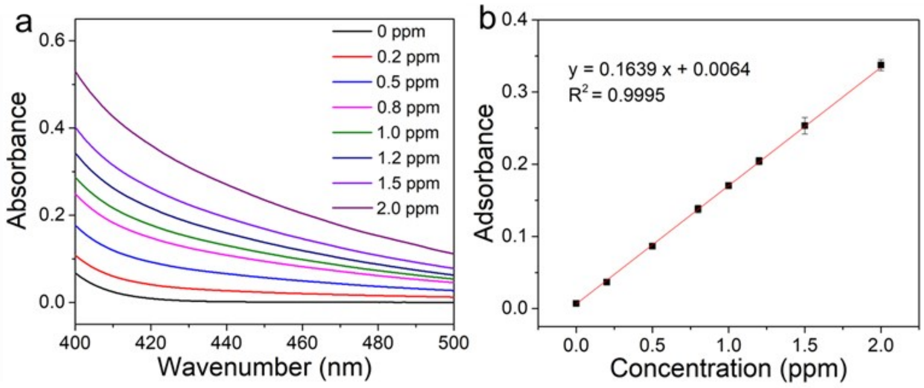

Fig. S13. (a) UV-Vis spectra of NH_4^+ standard solutions colored with Nessler's reagent after keeping in dark for 25 min at room temperature. (b) Calibration curve. The UV-Vis spectra were measured for three times and the average absorbance at 425 nm was taken to draw the curve.

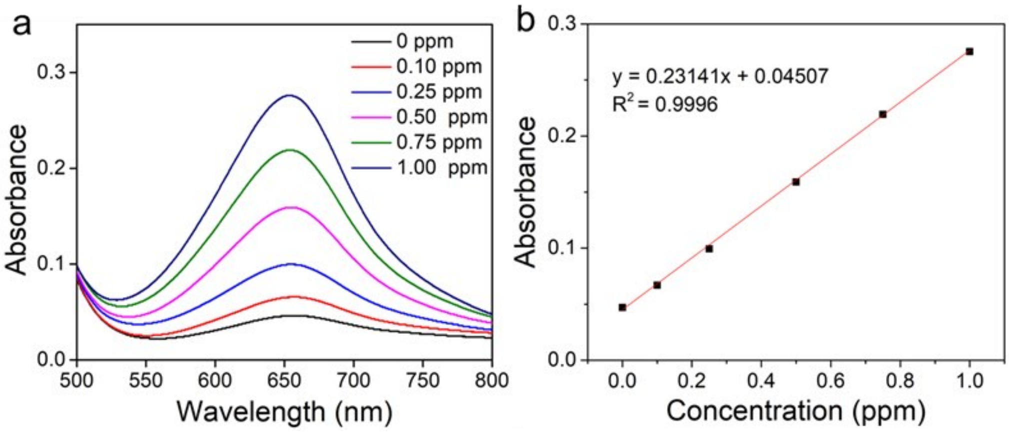

Fig. S14. (a) UV-vis curves of NH_4^+ standard solutions colored with indophenol blue after keeping in dark for 2 h at room temperature. (b) Calibration curve. The UV-Vis spectra were measured for three times and the average absorbance at 655 nm was taken to draw the curve.

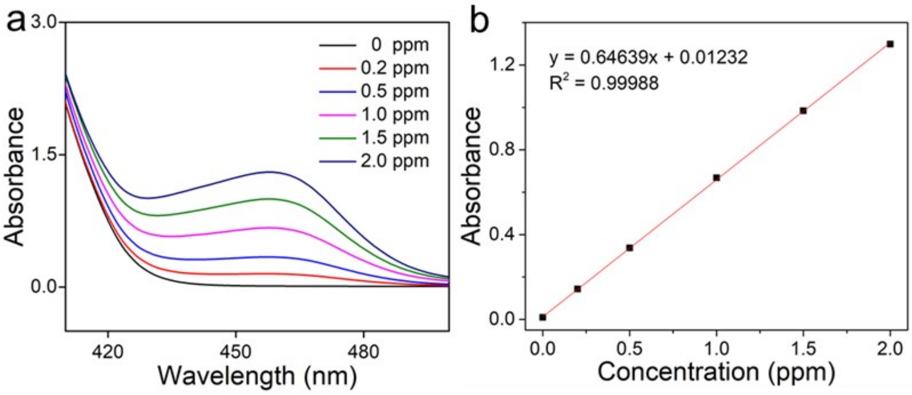

Fig. S15. (a) UV-vis curves of $N_2H_4{\cdot}H_2O$ standard solutions colored using Watt. and Chrisp method. (b) Calibration curve. The UV-Vis spectra were measured for three times and the average absorbance at 460 nm was taken to plot the curve.

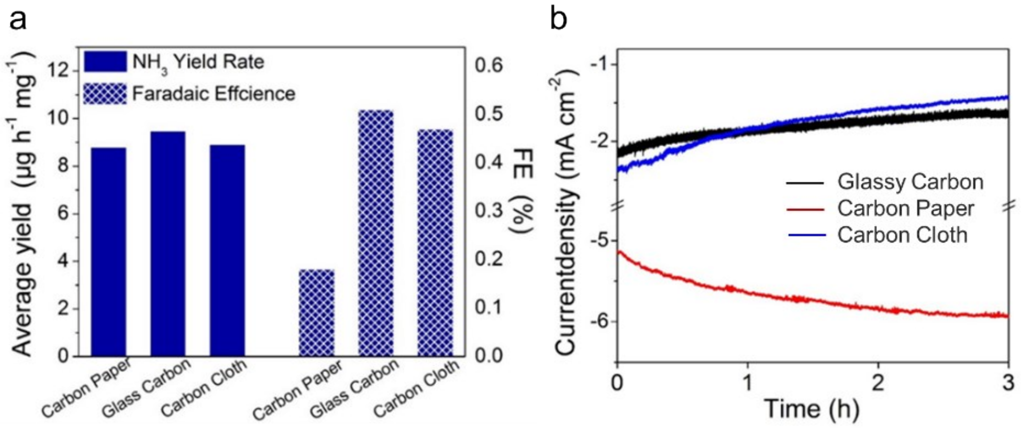

Fig.S16. (a) NH_3 yields and Faradaic efficiencies of Ru nanowires loaded on different substrates. (b) Chronoamperometry curves.

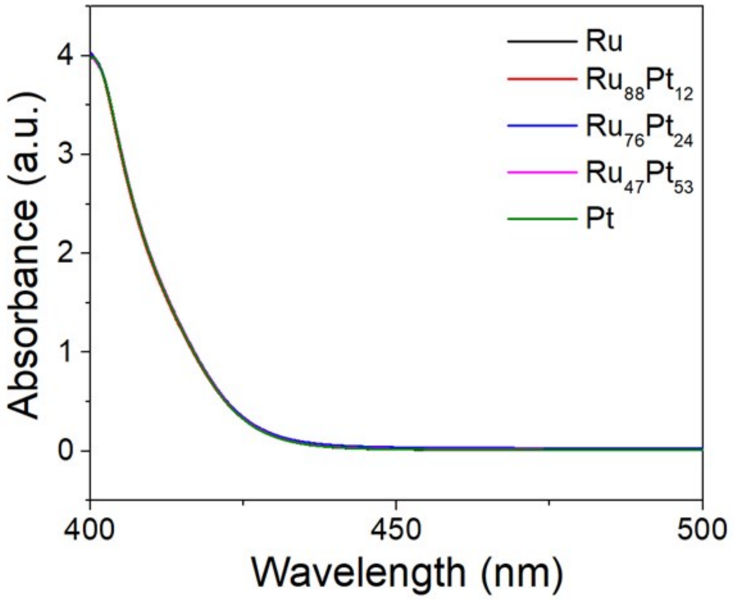

Fig. S17. UV-vis curves of the electrolytes collected after electrocatalysis by different catalysts at -0.2 V, which was colored using Watt. and Chrisp method.

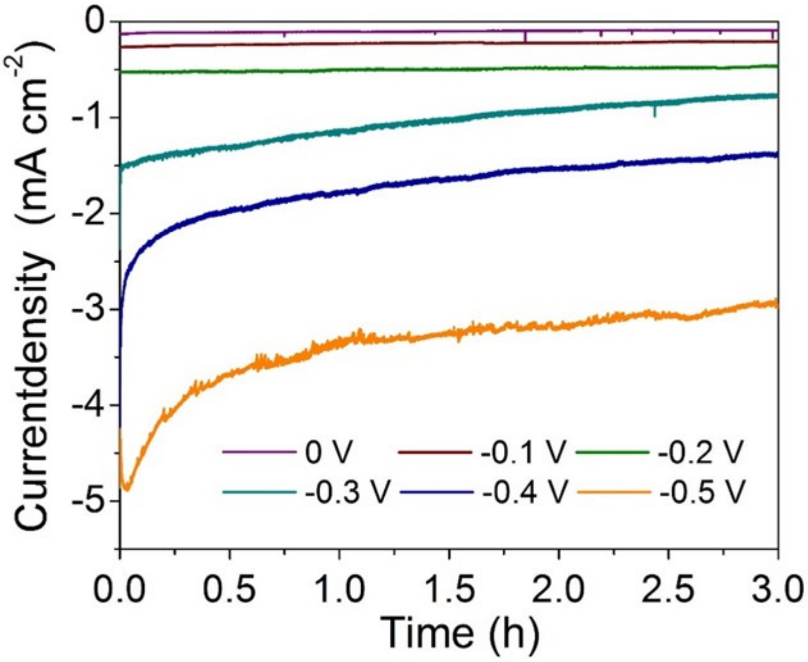

Fig. S18. Chronoamperometry curves of $Ru_{88}Pt_{12}$ nanowires obtained at different applied potentials with 3-h electrolysis.

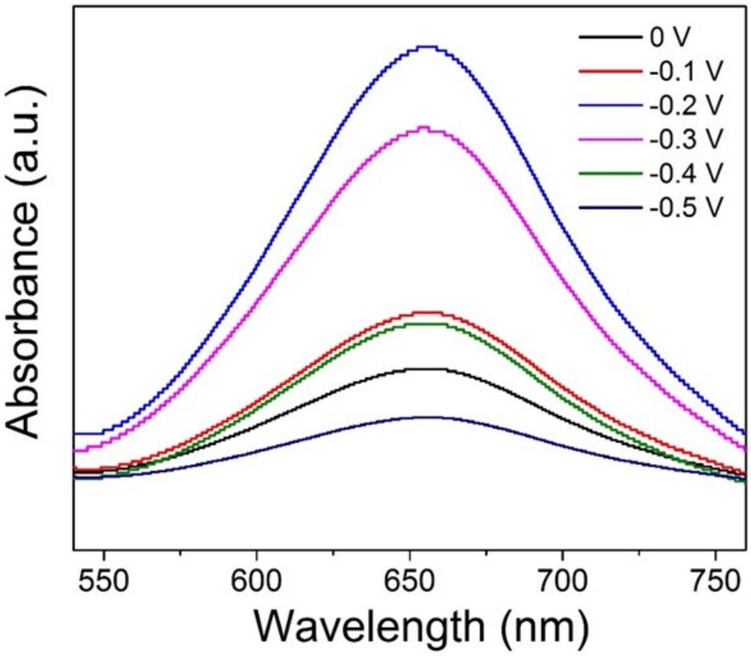

Fig. S19. The UV-Vis spectra of the electrolytes after electrocatalysis by $Ru_{88}Pt_{12}$ nanowires at different applied potentials.

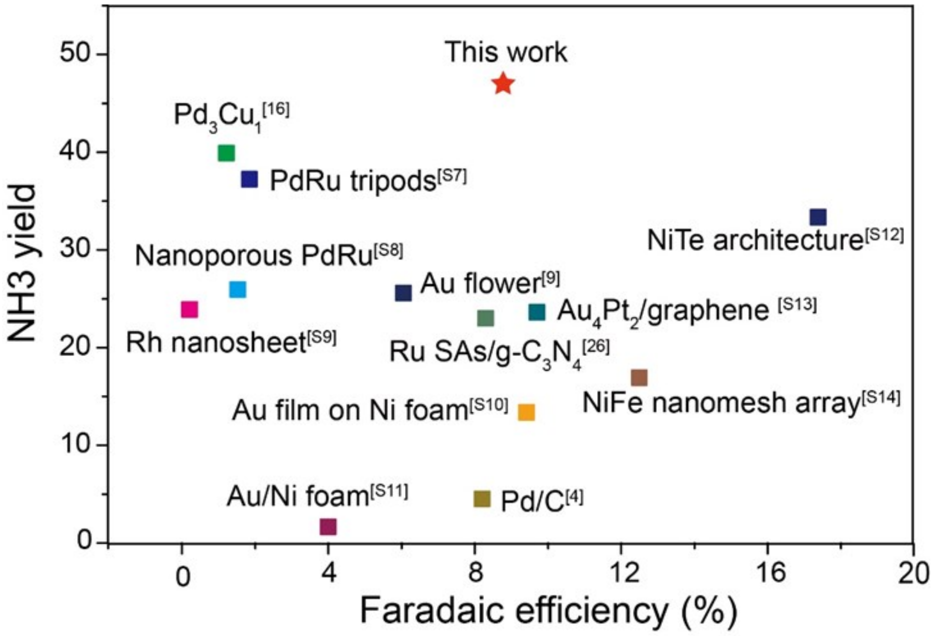

Fig. S20. Comparison of NH_3 yield and Faradaic efficiency between this work and other recent works.

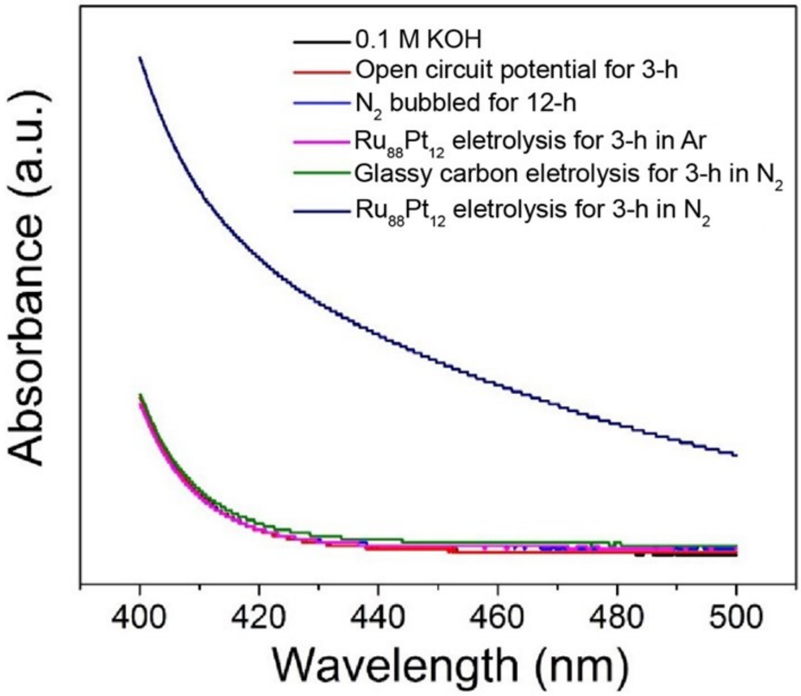

Fig. S21. UV-Vis spectra of the electrolytes after electrocatalysis at different conditions， which were colored by Nessler reagent method.

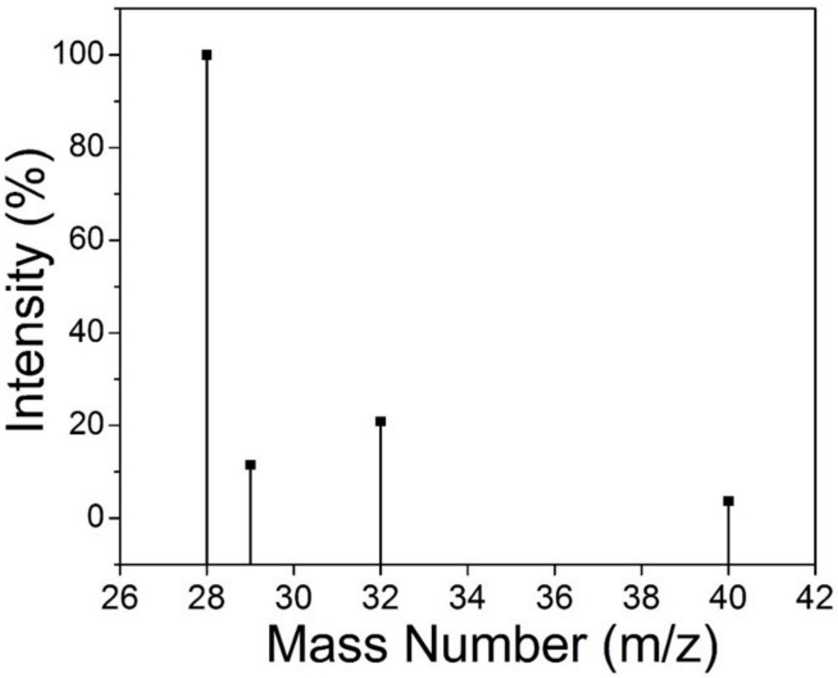

Fig. S22. The isotopic mass spectrometry of ^{15}N.

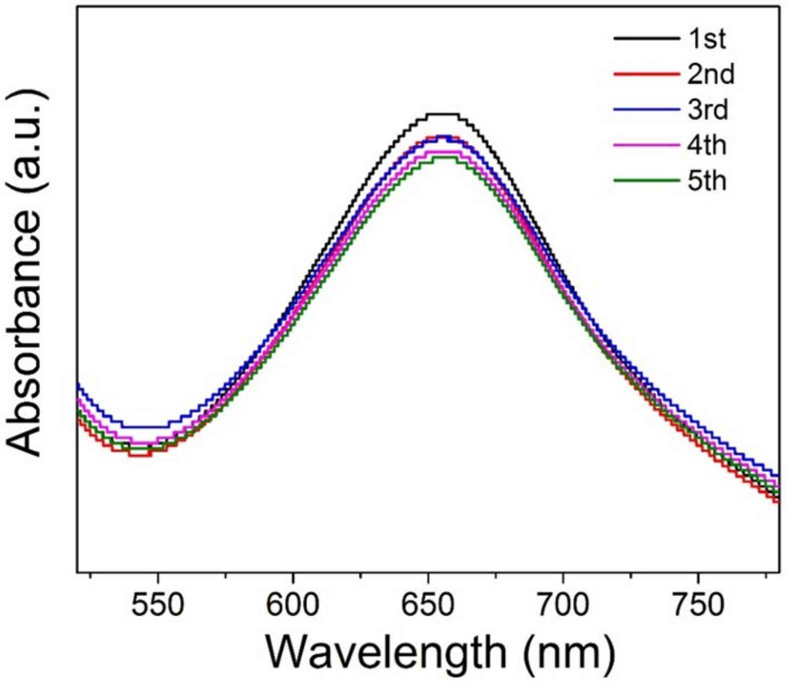

Fig. S23. UV-Vis spectra of the electrolytes collected after 5 consecutive cycles of ENRR electrolysis.

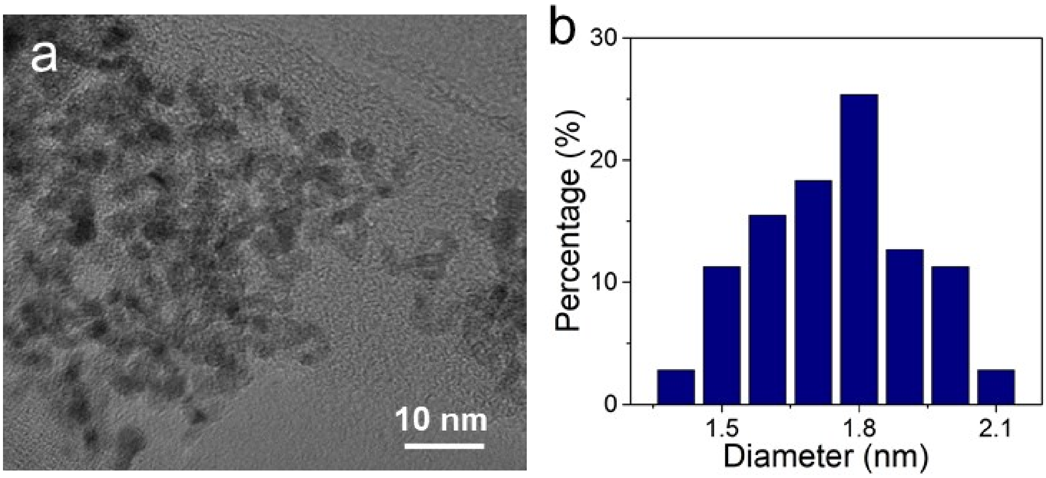

Fig. S24. (a) TEM image of $Ru_{88}Pt_{12}$ nanowires and (b) the diameter distributions of $Ru_{88}Pt_{12}$ nanowires (n=67) after 15 h ENRR electrolysis.

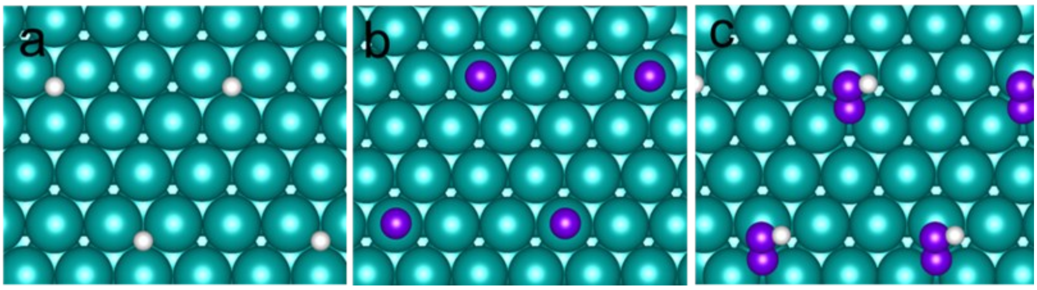

Fig. S25. The stable adsorption sites for adsorbents on Ru(111) surface: (a) H, (b) N_2, and (c) N_2H.

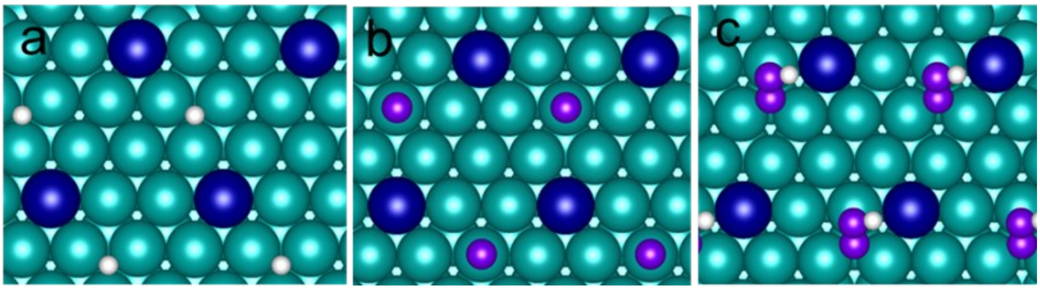

Fig. S26. The stable adsorption sites for adsorbents on Pt-decorated Ru(111) surface: (a) H, (b) N_2, and (c) N_2H.

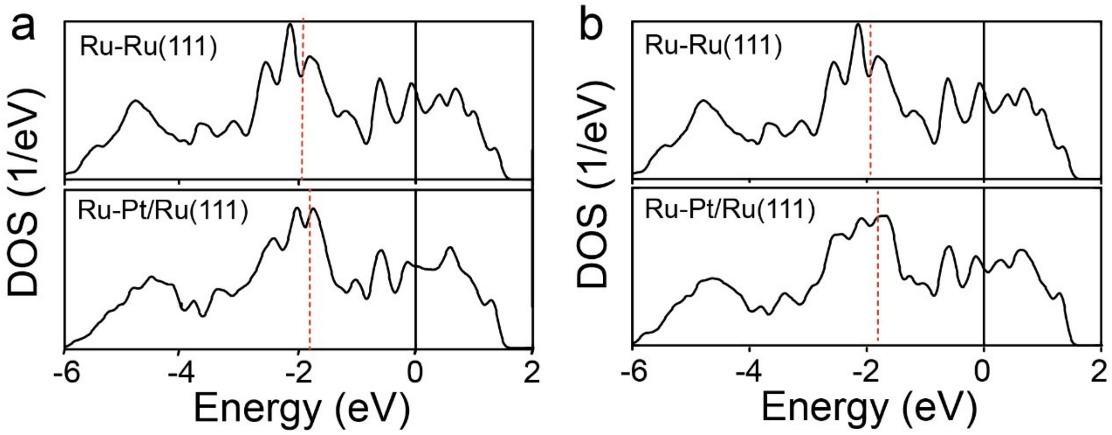

Fig. 27. Projected density of states for Ru atom 2 **(a)** and (b) atom 3 shown in Fig. 5a.

Table S1. The determined Pt/Ru atomic ratio and the corresponding feeding ratio of the metal precursors are consistent.

Catalysts	Feeding ratio of $RuCl_3$:H_2PtCl_6	Ru/Pt atomic ratio confirmed by ICP-MS
Ru	1:0	-
$Ru_{88}Pt_{12}$	6:1	88:12
$Ru_{76}Pt_{24}$	2.5:1	76:24
$Ru_{47}Pt_{53}$	1:1	47:53
Pt	0:1	-

Table S2. EXAFS fitting parameters at the Ru K-edge and Pt L_{III}-edge for various samples (S_0^2=0.807(Ru), 0.831(Pt)).

Sample	Shell	N^a	R(Å)^b	σ^2(Å^2)^c	ΔE_0(eV)^d	R factor
Ru K-edge						
Ru foil	Ru-Ru	12	2.67	0.0037	0.8	0.0094
RuO_2	Ru-O	6.0	1.98	0.0036	-2.5	0.0009
	Ru-Ru	1.8	3.12	0.0013		
	Ru-O	4.2	3.37	0.0036		
	Ru-Ru	3.8	3.56	0.0013		
Ru in $Ru_{88}Pt_{12}$	Ru-O	3.8	1.94	0.0069	-0.7	0.0018
	Ru-Ru	2.5	2.72	0.0067		
Pt L_{III}-edge						
Pt foil	Pt-Pt	12	2.76	0.0046	6.6	0.0014
PtO_2	Pt-O	6.0	2.02	0.0028	10.0	0.0008
	Pt-Pt	11.4	3.11	0.0052		
	Pt-O	7.5	3.17	0.0028		
Pt in $Ru_{88}Pt_{12}$	Pt-Ru	2.1	2.65	0.0018	6.4	0.0013
	Pt-Pt	6.5	2.74	0.0033		

[a]N: coordination numbers; [b]R: bond distance; [c]σ^2: Debye-Waller factors; [d] ΔE_0: the inner potential correction. R factor: goodness of fit. S_0^2 was set to 0.807 for Ru and 0.831 for Pt, according to the experimental EXAFS fit of Ru and Pt foil by fixing CN as the known crystallographic value.

References

[S1] J. Kong, A. Lim, C. Yoon, J.H. Jang, H.C. Ham, J. Han, S. Nam, D. Kim, Y.E. Sung, J. Choi, H.S. Park, Electrochemical synthesis of NH_3 at low temperature and atmospheric pressure using a γ-Fe_2O_3 catalyst, ACS Sustainable Chem. Eng. 5 (2017) 10986-10995.

[S2] G. Kresse, J. Furthmuller, Efficient iterative schemes for ab initio total-energy calculations using a plane-wave basis set. Phys. Rev. B 54 (1996) 11169-11186.

[S3] G. Kresse, D. Joubert, From ultrasoft pseudopotentials to the projector augmented-wave method. Phys. Rev. B 59 (1999) 1758-1775.

[S4] J. P. Perdew, K. Burke, M. Ernzerhof, Generalized gradient approximation made simple. Phys. Rev. Lett. 77 (1996) 3865-3868.

[S5] S. Grimme, Semiempirical GGA-type density functional constructed with a long-range dispersion correction. J. Comput. Chem. 27(2006) 1787-1799.

[S6] V. Barone, M. Casarin, D. Forrer, M. Pavone, M. Sambi, A. Vittadini, Role and effective treatment of dispersive forces in materials: polyethylene and graphite crystals as test cases. J. Comput. Chem. 30 (2009) 934-939.

[S7] H. Wang, Y. Li, C. Li, K. Deng, Z. Wang, Y. Xu, X. Li, H. Xue, L. Wang, One-pot synthesis of bi-metallic PdRu tripods as an efficient catalyst for electrocatalytic nitrogen reduction to ammonia, J. Mater. Chem. A 7 (2019) 801-805.

[S8] Z. Wang, C. Li, K. Deng, Y. Xu, H. Xue, X. Li, L. Wang, H. Wang, Ambient nitrogen reduction to ammonia electrocatalyzed by bimetallic PdRu porous nanostructures, ACS Sustainable Chem. Eng. 7 (2018) 2400-2405.

[S9] H.M. Liu, S.H. Han, Y. Zhao, Y.Y. Zhu, X.L. Tian, J.H. Zeng, J.X. Jiang, B.Y. Xia, Y. Chen, Surfactant-free atomically ultrathin rhodium nanosheet nanoassemblies for efficient nitrogen electroreduction, J. Mater. Chem. A 6 (2018) 3211-3217.

[S10] H. Wang, H. Yu, Z. Wang, Y. Li, Y. Xu, X. Li, H. Xue, L. Wang, Electrochemical fabrication of porous Au film on Ni foam for nitrogen reduction to ammonia, Small 15 (2019) e1804769.

[S11] D. Bao, Q. Zhang, F.L. Meng, H.X. Zhong, M.M. Shi, Y. Zhang, J.M. Yan, Q. Jiang, X.B. Zhang, Electrochemical reduction of N_2 under ambient conditions for artificial N_2 fixation and renewable energy storage using N_2/NH_3 cycle, Adv. Mater. 29 (2017) 1604799.

[S12] M. Yuan, Q. Li, J. Zhang, J. Wu, T. Zhao, Z. Liu, L. Zhou, H. He, B. Li, G. Zhang, Engineering surface atomic architecture of NiTe nanocrystals toward efficient electrochemical N_2 fixation, Adv. Funct. Mater. 2020, 10.1002/adfm.202004208.

[S13] C. Yao, N. Guo, S. Xi, C. Xu, W. Liu, X. Zhao, J. Li, H. Fang, J. Su, Z. Chen, H. Yan, Z, Qiu, P. Lyu, C. Chen, H. Xu, X. Peng, X. Li, B. Liu, C. Su, S. J. Pennycook, C.-J. Sun, J. Li, C. Zhang, Y. Du, J. Lu, Atomically-precise dopant-controlled single cluster catalysis for electrochemical nitrogen reduction, Nat. Commun. 11 (2020) 4389.

[S14] Y. Sun, T. Jiang, J. Duan, L. Jiang, X. Hu, H. Zhao, J. Zhu, S. Chen, X. Wang, Two-dimensional nanomesh arrays as bifunctional catalysts for N_2 electrolysis, 2020, DOI: 10.1021/acscatal.0c02745.